ACS APPLIED MATERIALS & INTERFACES

Research Article

www.acsami.org

Structural and Electronic Characterization of Nanocrystalline Diamondlike Carbon Thin Films

Neeraj Dwivedi,[†,‡] Sushil Kumar,*[,†] R. K. Tripathi,[†] J. D. Carey,[§] Hitendra K. Malik,[‡] and M. K. Dalai[†]

[†]National Physical Laboratory (CSIR), K.S. Krishnan Road, New Delhi 110 012, India

[‡]Department of Physics, Indian Institute of Technology Delhi, New Delhi 110 016, India

[§]Advanced Technology Institute, University of Surrey, Guildford, GU2 7XH, Surrey, United Kingdom

ABSTRACT: The origin of low threshold field-emission (threshold field 1.25 V/μm) in nanocrystalline diamond-like carbon (nc-DLC) thin films is examined. The introduction of nitrogen and thermal annealing are both observed to change the threshold field and these changes are correlated with changes to the film microstructure. A range of different techniques including micro-Raman and infrared spectroscopy, X-ray diffraction, electron microscopy, energy-dispersive X-ray analysis and time-of-flight-secondary ion mass spectroscopy are used to examine the properties of the films. A comparison of the field emission properties of nc-DLC films with atomically smooth amorphous DLC (a-DLC) films reveals that nc-DLC films have lower threshold fields. Our results show that nc-DLC can be a good candidate for large area field emission display panels and cold cathode emission devices.

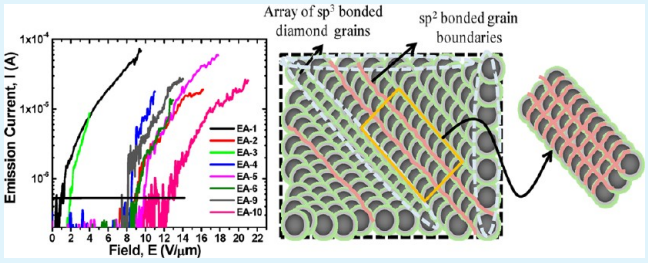

KEYWORDS: *diamondlike carbon, carbon nanostructures, field emission, threshold field, Raman spectroscopy, electron microscopy*

1. INTRODUCTION

Carbon-based materials have a number of properties that are attractive for large area electronic applications.[1−6] For example, diamond-like carbon can be deposited over large areas and at low substrate temperatures.[5] An important electronic property of such carbon-based materials, which includes diamond, carbon nanotubes (CNTs) and CNT-composites, is their ready ability to emit electrons into vacuum which make them suitable for applications in field emission display technology.[2,7,8] Diamond-like carbon (DLC) thin films are well-known for their exceptional mechanical properties[9−14] and recently, we have explored the mechanical, optical, and electrical properties of DLC and modified DLC thin films.[15−19] DLC thin films are known to emit electrons,[20,21] however, compared with diamond and CNTs, their threshold field (E_T) tends to be higher and emission current (I_E) is lower. As a consequence for the past few years research has been focused on nanocrystalline DLC (nc-DLC) films in order to reduce E_T and enhance I_E. If the value of E_T found in DLC and nc-DLC thin films could be engineered to be comparable to that of CNTs, this will be a major breakthrough for field-emission-based devices as the deposition of DLC and nc-DLC thin films over large area is a relatively simple and inexpensive process.

At present, the values of E_T reported from CNT cathodes vary from 1 to 5 V/μm.,[2,6,7] whereas E_T normally starts beyond 5 V/μm and can reach above 20 V/μm for DLC, tetrahedral amorphous carbon and nanodiamond thin films.[20−22] Ikeda and Teii[23] have demonstrated a low value of E_T of 3 V/μm in a nanocrystalline diamond field emitter. However, further reductions in E_T below 3 V/μm in DLC, modified DLC and nanodiamond films will be a great achievement toward the realization of simple, cheap and efficient field emission devices. In this paper, low threshold field emission ($E_T \approx 1.25$ V/μm) of electrons in simply fabricated nanocrystalline DLC (nc-DLC) films is demonstrated. In addition, the influence of nitrogen and vacuum annealing on the properties of modified nc-DLC thin films is also studied. The field emission characteristics of comparatively higher self-bias grown amorphous DLC (a-DLC) and nitrogen incorporated amorphous DLC (a-DLC:N) films are also studied and compared with the as grown and modified nc-DLC thin films.

2. MATERIALS AND METHODS

2.1. Sample Preparation. Radio frequency (13.56 MHz) plasma-enhanced chemical vapor deposition (RF-PECVD) is used for depositing the nanocrystalline diamondlike carbon (nc-DLC) and nitrogen incorporated nanocrystalline diamondlike carbon (nc-DLC:N) thin films over cleaned n-type silicon (Si) substrates at a base pressure of 1×10^{-5} Torr. The nc-DLC film is grown at a self-bias of −100 V (sample EA-1) by maintaining a working pressure of 2.4×10^{-3} Torr. This working pressure is obtained by first incorporating acetylene (C_2H_2) gas that changes the pressure from 10^{-5} Torr to 7.5×10^{-4} Torr and then argon (Ar) gas that changes the pressure from 7.5×10^{-4} Torr to 2.4×10^{-3} Torr. The nc-DLC:N thin film is deposited at a self-bias of −100 V (sample EA-2) with at a working pressure of 2.4×10^{-3} Torr, obtained by incorporating C_2H_2 and nitrogen (N_2) gases. Samples EA-3 and EA-5 are obtained when

Received: July 7, 2012
Accepted: September 20, 2012
Published: September 20, 2012

   dx.doi.org/10.1021/am301252e | *ACS Appl. Mater. Interfaces* 2012, 4, 5309−5316

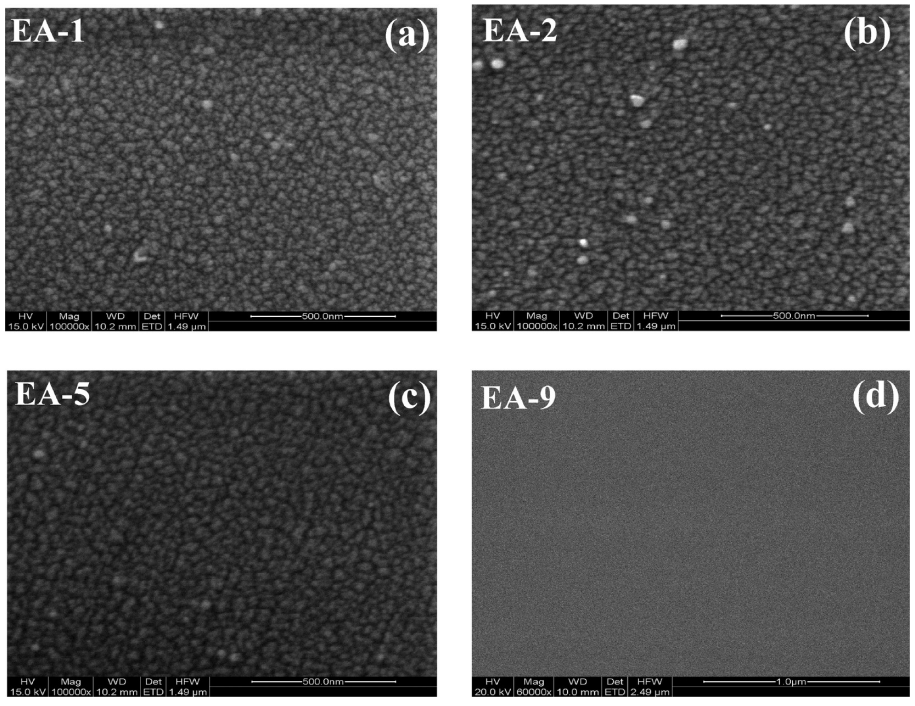

Figure 1. Scanning electron microscope images of (a) sample EA-1, (b) sample EA-2, (c) sample EA-5, and (d) sample EA-9.

sample EA-1 is annealed in a vacuum better than 1×10^{-5} Torr at 150 and 250 °C, respectively, for 90 min. Samples EA-4 and EA-6 are obtained when sample EA-2 is annealed at 150 and 250 °C, respectively, for 90 min. Besides nc-DLC films, amorphous DLC (a-DLC) and nitrogen incorporated a-DLC (a-DLC:N) films are also fabricated at comparatively higher self-bias of −180 V at a working pressure of 2.4×10^{-3} Torr. The a-DLC and a-DLC:N films grown at −180 V are labeled as samples EA-9 and EA-10, respectively.

2.2. Characterization of Samples. All of the films are characterized for their morphological, structural and field emission properties by field emission-scanning electron microscopy (FE-SEM) (FEI QUANTA 200 F), Raman spectroscopy (Reinshaw inVia Reflex micrometer Raman spectrometer attached with air cooled argon ion laser), X-ray diffraction (XRD) (Rigaku Miniflex II), Fourier transform infrared (FTIR) spectroscopy (Perkin-Elmer Spectrum BX), time-of-flight secondary ion mass spectroscopy (ToF-SIMS) (TOF-SIMS 5 of ION-TOF GmBH, Germany), Energy dispersive X-ray analysis (EDAX) and a Keithley software controlled I−V measurement unit (Keithley 2410), respectively. In addition, the optical and mechanical properties of the deposited films are investigated using ultraviolet spectroscopy (Shimadzu spectrophotometer) and nanoindentation (IBIS nanoindentation, M/S Fisher-Cripps laboratory, Australia), respectively. The field emission measurements are carried out at base pressure of 3×10^{-7} Torr. The threshold field is defined as the applied field at which an emission current of $\sim 5 \times 10^{-7}$ A is obtained. The micro-Raman measurements are performed using excitation wavelength of visible range (514.5 nm). ToF-SIMS measurements are conducted at ultrahigh vacuum condition with 5×10^{-10} mbar pressure, where pulsed primary ions from a 25 keV Bi liquid-metal ion gun (LMIG) are used to bombard the sample surface to create secondary ions. The sputtering is done using a 500 eV O_2 source to remove the first few layers from the sample surface. The sputtering and analysis area is 200×200 μm^2 and 70×70 μm^2, respectively, for all the samples. The overall resolution for ToF-SIMS is 1 nm.

3. RESULTS AND DISCUSSION

Figures 1a−1c show the FE-SEM images of samples EA-1, EA-2, and EA-5, respectively. The microscope images reveal nanostructured morphology with a uniform distribution of nanostructured carbon throughout the surface. A highly dense tightly packed structure is found in sample EA-1. However, when nitrogen introduction and annealing at 250 °C for 90 min in sample EA-1 are performed, slight changes into the structure of samples EA-2 and EA-5, respectively is observed. FE-SEM images of samples EA-2 and EA-5 clearly reveal the formation of nanocrystalline but images show no significant chages in the structure. The FESEM image of the a-DLC film (sample EA-9, Figure 1d), clearly confirms the amorphous morphology in that sample grown at higher self-bias.

The structural analysis of these samples is conducted using XRD with the recorded XRD patterns of samples EA-1 and EA-2 shown in panels a and b in Figure 2, respectively. The XRD spectra clearly reveal a mixture of nanocrystalline and amorphous carbon due to the presence of several sharp peaks as well as a broad band in the range of 10−60°. The peaks which appear in the range from 40 to 60° in sample EA-1 correspond to various reflections of the sp^3 diamond phase. Generally, nanodiamond films show a sharp and high intense diamond ⟨111⟩ peak at 43.9°. In contrast, sample EA-1 exhibits three peaks at 42.2, 45, and 46.6°, which are close to peak 43.9°. Bigelow et al.[24] have also found diamond peak at 45°. We expect that sample may have significant strain and these peaks are appeared as a consequence of strain induced spliting of ⟨111⟩ peak. The peak obtained at 53.6° also correspond to a diamond reflection.[25] The sharp peaks at 28.4, 31.1, 34.9, 47.6, and 56.4° are attributed to the silicon substrate.[25] The sharp peak generated at 38.4° may arise from SiC ⟨102⟩, which comes from a contribution of Si and C both at the interface.[25] Between 20 and 30°, the peaks are attributed to various reflections of sp^2-bonded graphitic material. A very sharp peak appeared at 26.6° corresponds to graphite ⟨111⟩. A broad band is seen centered around 22°, which shows the amorphous structure of the carbon bonding. In sample EA-2, all these peaks are slightly shifted to higher 2θ side due to nitrogen induced modification. This sample show sharp peaks at 27, 28.7, 31.4, 35.2, 38.6, 41.4, 42.4, 45.4, 46.7, 47.7, and 53.7°. Looking at the

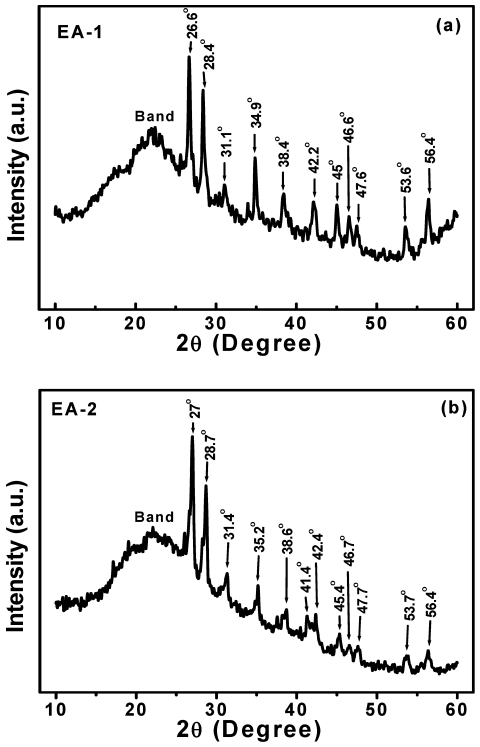

Figure 2. X-ray diffraction spectra of (a) sample EA-1 and (b) sample EA-2.

extra peak 41.4°; the peak at 42.4° in EA-1 splits into two peaks at 41.4° and 42.4° in EA-2 attributed to nitrogen induced modification. It is to be noted that the intensity of the sp^2-bonded band generated in the range 20−30° is found to be comparatively less intense and sp^3 bonded diamond peaks originated in the range 40−60° are found to be comparatively more intense in sample EA-1 than in sample EA-2. This suggests that sample EA-2 may have more sp^2 phase because of nitrogen introduction. Furthermore, an XRD spectrum of sample EA-9 is also recorded (not given here) that clearly confirms the creation of amorphous structure in this sample.

ToF-SIMS is a high-resolution destructive technique by which not only the constituents of films can be investigated but also atomic diffusion at the film/substrate interface can be visualized. Figure 3a−d shows the ToF-SIMS depth profiling of samples EA-1, EA-2, EA-5, and EA-6. It can be seen that C and H are found to be main constituents of samples EA-1 and EA-5, whereas C, H, and N are found to be main constituents of samples EA-2 and EA-6, which agrees with our deposition parameters. An intense peak corresponding to the Si substrate is evident in all four spectra. It is important to note that no oxygen appears in the film region, as the presence of oxygen is recorded only when depth profiling of substrate region begins. The presence of oxygen in the Si substrate is attributed to the fact that Czochralski (Cz)-Si wafer possesses oxygen as an impurity. The depth profile gives clear elemental demarcation between C, H, and Si in the case of samples EA-1 and EA-5 whereas C, H, N, and Si are evident in the case of samples EA-2 and EA-6. This can be seen in sample EA-1, where C and H diffuse slightly into the Si substrate but that H diffuses deeper because of its lower atomic weight. It is worth noting that the diffusion of C in sample EA-1 is found to be significantly lower than in unhydrogenated DLC and tetrahedral amorphous carbon (ta-C) films because of the presence of H. Furthermore, when sample EA-1 is annealed at 250 °C for 90 min, the diffusion of C and H is enhanced. Similarly based on analysis of samples EA-2 and EA-6, it is inferred that annealing at 250 °C for 90 min enhances the diffusion of C, H and N into the substrate. By taking the average intensity ratios, the

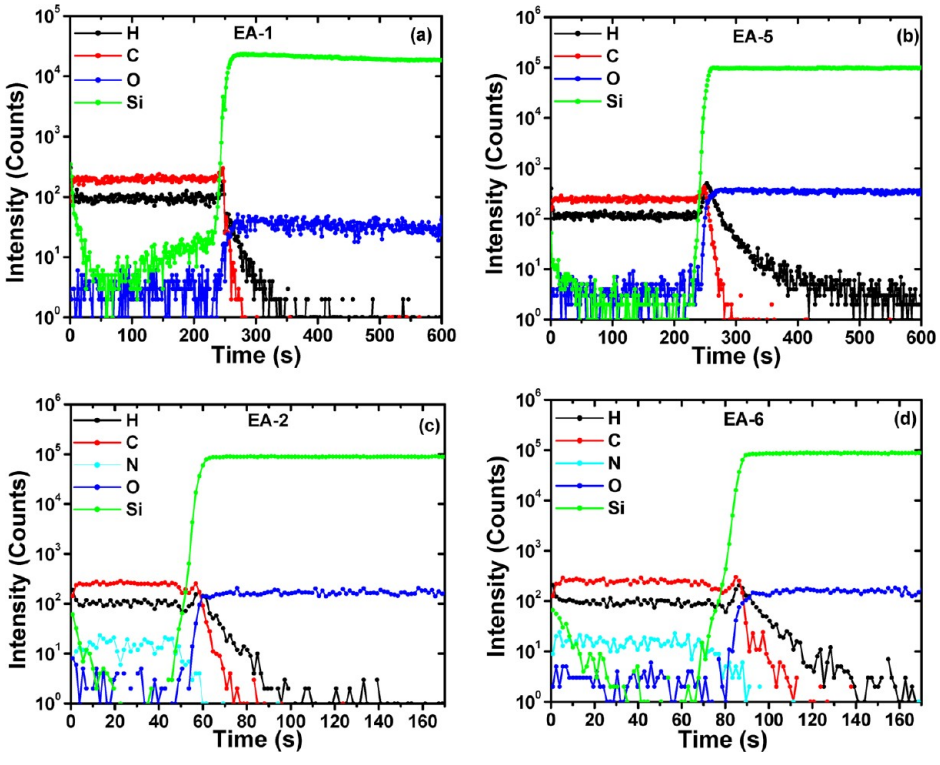

Figure 3. ToF-SIMS profiles of (a) sample EA-1, (b) sample EA-5, (c) sample EA-2, and (d) sample EA-6.

dx.doi.org/10.1021/am301252e | ACS Appl. Mater. Interfaces 2012, 4, 5309−5316

approximate percentage of nitrogen in a sample EA-2 has been estimated to be about 6 at %. This agrees well with the nitrogen content as estimated by EDAX. which is about 7 at %.

The micro-Raman spectra of nanocrystalline (samples EA-1, EA-2, EA-5, and EA-6) and amorphous (samples EA-9 and EA-10) DLC films are shown in Figure 4a. The visible (514.5 nm)

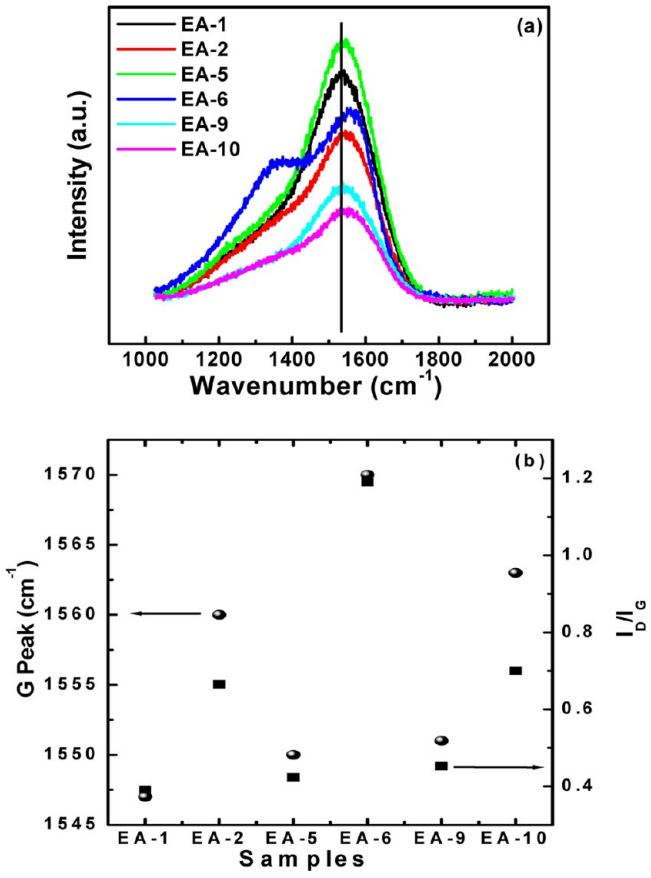

Figure 4. (a) Micro-Raman spectra of EA samples and (b) variation of G peak and I_D/I_G ratio for different samples.

Raman spectra of DLC films exhibit two bands, D (disorder) band near 1350 cm^{-1} and G (graphite) band near 1540 cm^{-1}. Visible Raman spectra are predominantly sensitive to sp^2 bonding due to the low energy separation. However, changes in G peak position and I_D/I_G ratios imply changes in carbon bonding and sp^2 carbon clustering. It is well-understood that an increase in G peak position from 1520 cm^{-1} to 1600 cm^{-1} and an increase in I_D/I_G ratio correspond to enhanced sp^2 bonding.[26] From Figure 4a, it is evident that the as-deposited samples EA-1 and EA-2 have not only a low D peak intensity (lower disorder) but also had G peak toward lower wavenumber. Among the two samples, sample EA-1 (nc-DLC film) has a lower disorder and G peak shifted toward lower wavenumber side than sample EA-2 (nc-DLC:N film). By contrast, annealing of the films leads to increased disorder with a shifting of the G peak toward higher wavenumber side in annealed samples EA-5 and EA-6. To get exact D and G peak position and their I_D/I_G ratios, the Raman spectra are fitted by considering two Gaussian components. The variations of G peak position and I_D/I_G ratio for different samples are given in Figure 4b, respectively. The position of G peak and I_D/I_G ratio in sample EA-1 is found to be 1547 cm^{-1} and 0.391, respectively, and 1560 cm^{-1} and 0.665, respectively, in sample EA-2. For the annealed samples, the position of the G peak and I_D/I_G ratio in sample EA-5 are found to be 1550 cm^{-1} and 0.424, respectively, whereas they are changed to 1570 cm^{-1} and 1.19, respectively, in sample EA-6. The nitrogen incorporation and annealing significantly affects the microstructure of these films by increasing the sp^2 phase. llie et al.[12] have also observed increased disorder and hence, enhanced I_D/I_G ratio in a-C:H, tetrahedral hydrogenated carbon (ta-C:H) and tetrahedral nitrogenated carbon (ta-C:N) thin films. Ferrari et al.[26,27] and Rodil et al.[28] have also suggested that the shifting of G peak toward higher wavenumber and increased I_D/I_G ratio in amorphous carbon films are accompanied by enhanced sp^2 bonding.

Our analysis also infers that thermal annealing had more pronounced behavior in nitrogen included nc-DLC:N films than pure nc-DLC films. This can be confirmed by analyzing the data of the as-deposited and annealed nc-DLC:N films with respect to the as-deposited and annealed nc-DLC film. The as-deposited nc-DLC:N film (sample EA-2) has a G peak at 1560 cm^{-1} but it is shifted by ~10 cm^{-1} toward higher wavenumber side in 250 °C annealed nc-DLC:N film (sample EA-6) and found to be at 1570 cm^{-1}. Similarly, the I_D/I_G ratio in sample EA-2 is found to be 0.665, which is larger than the value of 0.12 in sample EA-6. By contrast, the as-deposited nc-DLC film (sample EA-1) had a G peak at 1547 cm^{-1} which is shifted by only 3 cm^{-1} toward higher wavenumber side in 250 °C annealed nc-DLC film (sample EA-5) and found to be at 1550 cm^{-1}. The I_D/I_G ratio in sample EA-1 is found to be 0.39, which is increased to 0.42 in sample EA-5.

Temperature-induced structural transformation are more pronounced in nc-DLC:N film and give rise to the creation of more sp^2 bonding in annealed nc-DLC:N film (sample EA-6). The G peak position and I_D/I_G ratio in comparatively higher self-bias deposited a-DLC film (sample EA-9) are found at 1551 cm^{-1} and 0.453, respectively. These are increased to 1563 cm^{-1} and 0.7, respectively, in a-DLC:N film (sample EA-10) due to nitrogen driven enhanced sp^2 bonding. The difference in the G peak position and I_D/I_G ratio between −100 V and −180 V self-bias grown nc-DLC and a-DLC; nc-DLC:N and a-DLC:N films are found to be small which suggests that at a higher self-bias of −180 V an increase in sp^2 bonding takes place. FTIR is found to be an important tool for investigating the bonding environment of DLC and modified DLC thin films. Figures 5a, b show the FTIR spectra of sample EA-1 and EA-2 in the range 1200−2200 cm^{-1} and 2700−3500 cm^{-1}, respectively. Sample EA-1, which is a pure nc-DLC film, shows various vibrating modes such as the $C-H_n$ stretching mode in the range 2700−3150 cm^{-1}, $C-H_n$ bending mode (or olefinic mode) in the range 1300−1550 cm^{-1}. The FTIR spectra also shows an important peak corresponding to C═C vibrations in the band 1560 −1660 cm^{-1} and OH bonding above 3200 cm^{-1}. When nitrogen is introduced in nc-DLC film, two changes are realized in the nc-DLC:N film (sample EA-2). First, the intensity of the peak in the range 1560 - 1660 cm^{-1} is significant increased, which is attributed to nitrogen introduction promoting the formation of C═N bonding (enhanced sp^2 bonding). Second, the intensity of the $C-H_n$ stretching vibrations is reduced, which is due to the fact that nitrogen inclusion may replace some of the C atoms in $C-H_n$ stretching vibrations and generate N−H-based bonding above 3150 cm^{-1}. The optical and nanomechanical properties of these EA samples are examined and discussed in brief here. Sample EA-1 with an optical band gap of 1.7 eV shows highest hardness

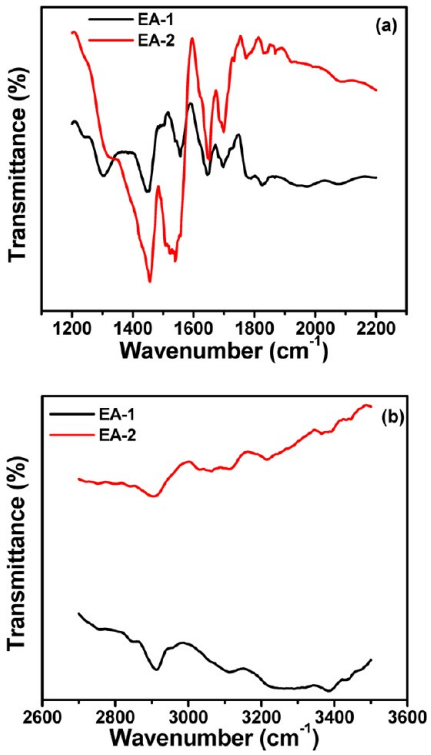

Figure 5. FTIR spectra of samples EA-1 and EA-2 in the ranges (a) 1200−2200 cm^{-1} and (b) 2700−3500 cm^{-1}.

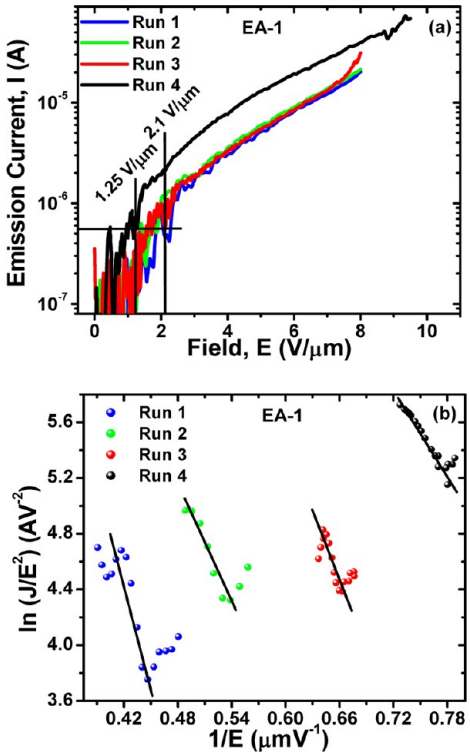

Figure 6. (a) Field-emission $I-E$ curves of sample EA-1 taken at different runs and (b) Fowler−Nordheim plots of sample EA-1 for different runs.

as 35.8 GPa. However, introduction of nitrogen, annealing and increase in self-bias leads to reduction of hardness due to enhanced sp^2 bonding. The optical property also supports the increase in sp^2 bonding due to introduction of nitrogen because optical band gap in sample EA-2 reduces to 1.1 eV. Thus, optical and nanomechanical properties infer that sample EA-1 possesses more sp^3 bonding because of its higher hardness and large band gap.

The field emission current (I) versus field (E) curves of sample EA-1 recorded over various successive cycles are shown in Figure 6a. Moving from run 1 to run 4, the threshold field is found to reduce from ∼2.1 V/μm to 1.25 V/μm. Not only this, the emission current (I_E) is also found to be highest in run 4. The recorded I-E characteristics of sample EA-1 in various runs are fitted with a Fowler-Nordheim (F−N) model in Figure 6b, where a plot of ln (J/E^2) versus $1/E$ is shown. The F−N theory is related to the emission of electrons from the front surface via tunneling[5,29] through an approximately triangular barrier. The Fowler-Nordheim equation takes the form

$$J = \frac{a(\beta E)^2}{\phi}\exp\left(\frac{-b\phi^{3/2}}{\beta E}\right) \quad (1)$$

where J is the current density, Φ is the potential barrier height (taken as the work function), E is the applied (or macroscopic) electric field, β is the field enhancement factor, and a and b are constants and have the values of 1.56×10^{-6} A eV V^{-2} and 6.83×10^7 V eV$^{-3/2}$ cm^{-1}, respectively. It can be seen that these emission curves are well-fitted in their F−N plots, confirming that the electrons are emitted by cold cathode emission process. With the help of such F−N plots, the field-enhancement factor (β) can be estimated for a given value of Φ, taken as 5 eV. The parameter β is associated with the generation of the local field rather than the applied field and is normally expressed in terms of ratio of local (E_{local}) to applied (E) field. If β is large then lower applied fields can generate same the high local fields necessary for good field emission. The value of β is found to vary from 7620 to 8962 for sample EA-1 from run 1 to run 4 which explains the reduction in the threshold applied field.

Depending upon film structure, two types of field-emission mechanisms are possible in amorphous and nanostructured carbon films. Generally low bias grown polymerlike amorphous carbon (PAC) films with fewer defects and low conductivity show back contact controlled field emission due to the formation of leaky barrier at the film/back contact interface. In contrast, comparatively higher self-bias grown DLC and nc-DLC films having high defect density and higher the conductivity exhibit front surface based emission.[5] Various models have been suggested with regard to the explanation of field emission from DLC thin films, but a complete interpretation remains unresolved. The situation becomes difficult when E_T reaches below 5 V/μm; Ikeda and Teii[23] have observed a low value of $E_T \sim 3$ V/μm in nanodiamond films and suggested a possible reason based on defect-induced conduction that becomes stronger under nitrogen inclusion. Previously Carey et al.[30] had suggested that defect and localized states near the Fermi level in the form of sp^2 clusters in the sp^3 matrix help to obtain efficient field emission with E_T below 10 V/μm. Normally, sp^2 clusters in DLC films are distributed in the sp^3 matrix; in diamond and polycrystalline diamond films the conducting sp^2 bonded grain boundaries surround the sp^3 bonded grains. The same explanation used for diamond and polycrystalline diamond is also applicable for the present nc-DLC film (or nanodiamond film sample EA-1), where sp^3 bonded nanodiamond grains are bordered with sp^2 bonded grain boundries. However, in contrast to diamond and polycrystalline diamond films, nc-DLC or nanodiamond film

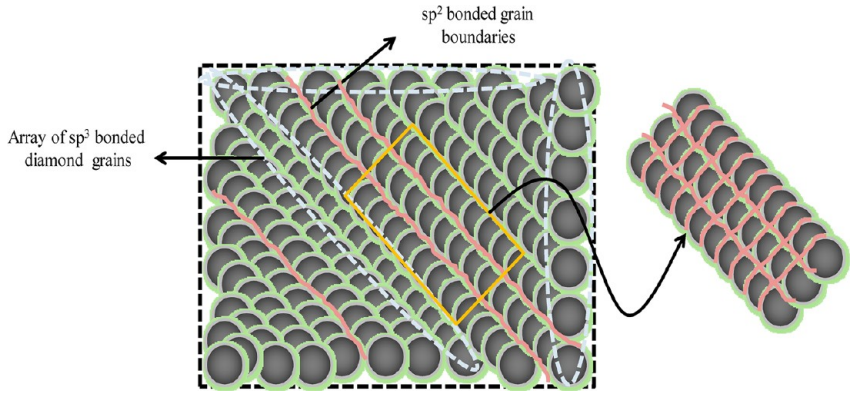

Figure 7. Proposed model where diamond grains are considered as dielectric regions and graphite grain boundaries are considered as conducting pathways.

possesses more grain boundaries. Since diamond grains with sp^3 bonding exhibit low and even negative electron affinity (NEA), the electrons see a negligible potential barrier for emission and are emitted at lower E_T. Under the action of an external field, a large local field will be generated around the sp^2-bonded grain boundaries due to termination of the field lines. As a result both sp^2 bonding and sp^3 bonding play an important role for field emission from nc-DLC films.

Optimum values of sp^3 and sp^2 bonding are needed for optimum field-emission from nc-DLC films. It is important to mention that in contrast to unhydrogenated counterpart, hydrogenated DLC and nc-DLC film (with certain amount of hydrogen) exhibit high sp^3 bonding as well as low electron affinity. Since a low value of E_T is realized in sample EA-1, a possible model pertaining to explain the field emission behavior is schematically depicted in Figure 7. In present model, we refer sp^2-bonded conducting grain boundaries as a 'conducting pathway' and the surrounding sp^3-bonded nanodiamond grains are treated as dielectric (insulator/semiconductor) regions. These sp^2 bonded conducting pathways may have a high-aspect- ratio forming an effective percolating network pathway in the film. Recently, Varshney et al.[31] have fabricated a diamond and CNT composite structure and observed low E_T and high I_E characteristics during field emission measurement. They have suggested that CNTs have a high aspect ratio and during field emission heat is produced in CNTs. The sp^3 diamond grains act as a heat sink and help to maintain the efficient field emission property of overall structure. Similarly in sample EA-1, under the action of an external field the sp^2-bonded conducting pathways may be heated due to predominant emission of electrons through this region. Among the four runs, run 4 exhibit lowest E_T and highest I_E; attributed to current induced transformation of sp^3 bonding into sp^2 bonding.[32]

To explore the influence of nitrogen incorporation and annealing on the field-emission characteristics of nc-DLC and modified nc-DLC films, the field-emission $I-E$ curves of different nc-DLC based devices are recorded (samples EA-1 to EA-6), as shown in Figure 8a. Here, it is found that among all samples, the sample EA-1 shows lowest E_T at 1.25 V/μm. However, when sample EA-1 is annealed at 150 °C for 90 min, the value of E_T in sample EA-3 is slightly increased to 1.76 V/μm. Nevertheless, when the temperature for annealing of sample EA-1 is increased to 250 °C (for 90 min), the value of E_T in sample EA-5 is drastically enhanced to 9.8 V/μm, which is found to be the highest E_T among all the nc-DLC samples. This

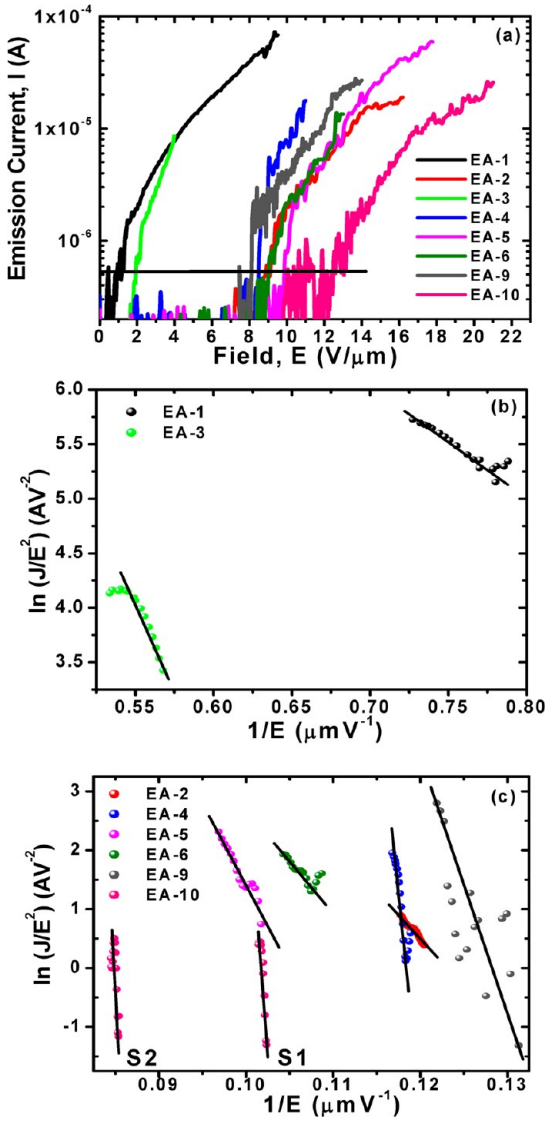

Figure 8. (a) Field-emission $I-E$ curves of different EA samples and (b) F–N plots of EA samples and (c) F–N plots of samples EA-1, EA-2, EA-3, EA-4, EA-5, EA-6, EA-9, and EA-10.

infers that annealing of these nc-DLC films modifies the film structure and affects the electron emission. On the basis of a change of 0.51 V/μm in E_T between samples EA-1 and EA-3, it

dx.doi.org/10.1021/am301252e | ACS Appl. Mater. Interfaces 2012, 4, 5309–5316

is realized that annealing at low temperature (150 °C) has a less pronounced effect on field emission properties of nc-DLC films. When annealing temperature is raised to 250 °C, the structure of the film gets changed considerably (e.g., the generation of more sp^2 clustering as confirmed by Raman analysis and the enhanced diffusion of atoms as measured by ToF-SIMS) that causes the largest shift of E_T of 8.6 V/μm between samples EA-1 and EA-5. When nitrogen is introduced, the value of E_T in sample EA-2 is significantly increased to 8.3 V/μm. This is due to the fact that introduction of nitrogen significantly modifies the structure of resulting sample EA-2 and increases the sp^2 bonding, as confirmed by Raman and FTIR analyses. Furthermore, when sample EA-2 is annealed at 150 and 250 °C for 90 min, the value of E_T in samples EA-4 and EA-6 is increased to 8.4 and 9.2 V/μm, respectively.

Not only the value of E_T but also the magnitude of maximum I_E varied significantly with the changing annealing temperature and the introduction of nitrogen. We believe that the annealing and nitrogen inclusion disturbs the optimum ratio of sp^3-bonded dielectric regions (nanograins) and sp^2-bonded conducting pathways (grains boundaries) and hence, enhanced the E_T and lower I_E. The increased value of E_T in samples EA-5 and EA-6 are also correlated with interdiffusion of C, H and N into Si as studied by ToF-SIMS. As annealing of sample EA-1 at 250 °C leads to enhanced diffusion of C and H elements into Si, which results in large mismatches at the interface and hence, contribute enhancing the value of E_T of sample EA-5. Similarly, annealing of sample EA-2 at 250 °C enhanced the diffusion of C, H and N species into Si that further enhances the interfacial mismatch and therefore, helps increasing the E_T of resultant sample EA-6. The interdiffusion of these elements may also disturb the electrical characteristics of the back contact making the back contact more resistive explaining the large values of E_T obtained in annealed samples than that of as-deposited samples.

The influence of morphology and self-bias on field emission property of carbon films are also explored. The I-E characteristics of a-DLC (sample EA-9) and a-DLC:N films (sample EA-10) are recorded is shown in Figure 8a. The value of E_T and the maximum value of I_E in a-DLC film (sample EA-9) are found to be 7.6 V/μm and 2.7×10^{-5} A, respectively. On the other hand, a-DLC:N film exhibits a comparatively higher vaue of E_T and lower current. In sample EA-10 initial emission begins at 9.77 V/μm which is higher than the value of E_T of sample EA-9 due to nitrogen induced structural changes as confirmed by micro-Raman analysis. When compared the values of E_T of sample EA-9 with EA-1, the value of E_T is found to be significantly larger in EA-9, which is due to fact that EA-1 possess nanostructure (some geometrical structure that helps enhancing local field), whereas EA-9 shows an amorphous structure (no geometrical enhancement). Similarly, the value of E_T of EA-10 is found to be larger than that of EA-2 due to the amorphous structure and higher self-bias growth of former sample.

Examining the current research on carbon based materials for field emission applications; Talapatra et al.[2] have demonstrated the lowest E_T as 3.22 V/μm in his MWCNT sample. On the other hand, Varshney et al.[7] have obtained a low value of E_T as 2.4 V/μm in a complex graphene-diamond hybrid film. They have also reduced E_T to 1.1 V/μm (at a current $\sim 1 \times 10^{-8}$ A) in complex and expensive nanotube/diamond composite[31] but the value of E_T in this sample is found to be 4 V/μm at current $\sim 10^{-5}$ A. They have also observed E_T of 5−6 V/μm in complex rod-shaped DLC nanostructures.[33] Shimada et al.[34] have also observed low E_T as ~3 V/μm in their complex and unconventional carbon nanowalls structure. Moreover Ikeda and Teii[23] have realized E_T as 3 V/μm in nanocrystalline diamond. In our case of nc-DLC film (sample EA-1) the value of E_T of 1.25 V/μm must be seem to be very encouraging. All the I-E characteristics of the samples are fitted to F−N plots. F−N plots of samples EA-2, EA-4, EA-5, EA-6, EA-9, and EA-10 overlap each other; hence, we have sketched F−N plots of samples EA-1 and EA-3 separately, which as shown in Figure 8b and F−N plots of samples EA-2, EA-4, EA-5, EA-6, EA-9, and EA-10 are given in Figure 8c. Here all emission curves properly fitted for F−N plots confirming electrons are emitted from the front surface. It is to be noted that sample EA-10 possesses two slopes, one in low field and other in comparatively higher field, as represented by S1 and S2, respectivel,y which usually signifies the presence of current saturation at the higher field values.[8]

4. CONCLUSIONS

In conclusion, we have demonstrated low threshold field emission in a simple and inexpensive nanocrystalline DLC thin film. We have explained the data in terms of model based on conducting pathways of sp^2 bonded carbon surrounded by dielectric regions of sp^3-bonded carbon. We believe that this lowest threshold field could be obtained from an optimum amount of sp^3 and sp^2 bonding. The addition of nitrogen and thermal annealing both results in increased value of threshold field, which was attributed to the introduction of increased disorder and enhanced interdiffusion of C and H species into the substrate Si. The effects of self-bias and surface morphology have also been examined. Compared with −100 V deposited nanocrystalline counterpart, the threshold field is found to be higher in higher self-bias deposited amorphous DLC and nitrogenated amorphous DLC thin films. Owing to excellent field emission characteristic with low threshold field, nc-DLC films have great potential for large area electronic devices.

AUTHOR INFORMATION

Corresponding Author

*Tel.: +91 11 45608650. Fax: +91 11 45609310. E-mail: skumar@nplindia.org.

Notes

The authors declare no competing financial interest.

ACKNOWLEDGMENTS

The authors are grateful to the Director, National Physical Laboratory, New Delhi (India) for his kind support. The authors wish to thank Mr. Ishpal, Ms. Kalpana Lodhi, Ms. Geetanjali Sehgal, Mr. C. M. S. Rauthan and Dr. O. S. Panwar for their help. ND acknowledges CSIR, Govt. of India for providing financial support through SRF fellowship. CSIR, Govt. of India is also acknowledged for rendering a Network Project NWP-0027.

REFERENCES

(1) Mochalin, V. M.; Shenderova, O.; Ho, D.; Gogotsi, Y. *Nat. Nanotechnol.* **2012**, *7*, 11.

(2) Talapatra, S.; Kar, S.; Pal, S. K.; Vajtai, R.; Cl, L.; Victor, P.; Shaijumon, M. M.; Kaur, S.; Nalamasu, O.; Ajayan, P. M. *Nat. Nanotechnol.* **2006**, *1*, 112.

(3) Bhattacharyya, S.; Henley, S. J.; Mendoza, E.; Rojas, L. G.; Allam, J.; Silva, S. R. P. *Nat. Mater.* **2006**, *5*, 19.

(4) Wu, Y.; Lin, Y. M.; Bol, A. A.; Jenkins, K. A.; Xia, F.; Farmer, D. B.; Zhu, Y.; Avouris, P. *Nature* **2011**, *472*, 74.
(5) Carey, J. D. *Philos. Trans. R. Soc. London, Ser. A* **2003**, *361*, 2891.
(6) Biswas, C.; Lee, Y. H. *Adv. Funct. Mater.* **2011**, *21*, 3806.
(7) Varshney, D.; Rao, C. V.; Guinel, M. J. F.; Ishikawa, Y.; Weiner, B. R.; Morell, G. *J. Appl. Phys.* **2011**, *110*, 044324.
(8) Connolly, T.; Smith, R. C.; Hernandez, Y.; Gun'ko, Y.; Coleman, J. N.; Carey, J. D. *Small* **2009**, *5*, 826.
(9) Robertson, J. *Semicond. Sci. Technol.* **2003**, *18*, 12.
(10) Schwan, J.; Batori, V.; Ulrich, S.; Ehrhardt, H.; Silva, S. R. P. *J. Appl. Phys.* **1998**, *84*, 2071.
(11) Silva, S. R. P.; Robertson, J.; Amaratunga, G. A. J.; Rafferty, B.; Brown, L. M.; Schwan, J.; Franceschini, D. F.; Marriotto, G. *J. Appl. Phys.* **1997**, *81*, 2626.
(12) Ilie, A.; Ferrari, A. C.; Yagi, T.; Rodil, S. E.; Robertson, J.; Barborini, E.; Milani, P. *J. Appl. Phys.* **2001**, *90*, 2024.
(13) Konofaos, N.; Thomas, C. B. *Appl. Phys. Lett.* **1992**, *61*, 2805.
(14) Godet, C.; Conway, N. M. J.; Bouree, J. E.; Bouamra, K.; Grosman, A.; Ortega, C. *J. Appl. Phys.* **2002**, *91*, 4154.
(15) Dwivedi, N.; Kumar, S.; Malik, H. K. *J. Appl. Phys.* **2012**, *111*, 014908.
(16) Dwivedi, N.; Kumar, S.; Malik, H. K. *ACS Appl. Mater. Interfaces* **2011**, *3*, 4268.
(17) Dwivedi, N.; Kumar, S.; Malik, H. K. *Solar Energy* **2012**, *86*, 220.
(18) Dwivedi, N.; Kumar, S.; Tripathi, R. K.; Malik, H. K.; Panwar, O. S. *Appl. Phys. A: Mater. Sci. Process.* **2011**, *105*, 417.
(19) Dwivedi, N.; Kumar, S.; Rauthan, C. M. S.; Panwar, O. S. *Plasma Process. Polym.* **2011**, *8*, 100.
(20) Carey, J. D.; Forrest, R. D.; Khan, R. U. A.; Silva, S. R. P. *Appl. Phys. Lett.* **2000**, *77*, 2006.
(21) Carey, J. D.; Smith, R. C.; Silva, S. R. P. *J. Mater. Sci.: Mater. Electron.* **2006**, *17*, 405.
(22) Forest, R. D.; Burden, A. P.; Silva, S. R. P.; Cheah, L. K.; Shi, X. *Appl. Phys. Lett.* **1998**, *73*, 3784.
(23) Ikeda, T.; Teii, K. *Appl. Phys. Lett.* **2009**, *94*, 143102.
(24) Bigelow, L. K.; Ellison, C.; Gunderson, D.; Hoggins, J. T. U. S. Patent 1993, Documents 4434188, 4507588, 4585668, 4591662, 4630566.
(25) Standard data, JCPDS Card numbers 791473, 791471, 791470, 731664, 752078 and 791715.
(26) Ferrari, A. C.; Robertson, J. *Philos. Trans. R. Soc. London, Ser. A* **2004**, *362*, 2477.
(27) Ferrari, A. C.; Rodil, S. E.; Robertson, J. *Phys. Rev. B* **2003**, *67*, 155306.
(28) Rodil, S. E.; Ferrari, A. C.; Robertson, J.; Milne, W. I. *J. Appl. Phys.* **2001**, *89*, 5425.
(29) Fowler, R. H.; Nordheim, L. *Proc. R. Soc. London, Ser. A* **1928**, *119*, 173.
(30) Carey, J. D.; Forrest, R. D.; Silva, S. R. P. *Appl. Phy. Lett.* **2001**, *78*, 2339.
(31) Varshney, D.; Weiner, B. R.; Morell, G. *Carbon* **2010**, *48*, 3353.
(32) Carey, J. D.; Silva, S. R. P. *Appl. Phys. Lett.* **2001**, *78*, 347.
(33) Varshney, D.; Makarov, V. I.; Saxena, P.; Berrios, A. G.; Scott, J. F.; Weiner, B. R.; Morell, G. *Nanotechnology* **2010**, *21*, 285301.
(34) Shimada, S.; Teii, K.; Nakashima, M. *Diamond Relat. Mater.* **2010**, *19*, 956.